C.P.Anil Kumar, et.al, International Journal of Engineering Research and Applications
www.ijera.com
ISSN: 2248-9622, Vol. 15, Issue 5, May 2025, pp 158-171

RESEARCH ARTICLE OPEN ACCESS

Modelling and Forecasting Fair-Weather Atmospheric Electric Field using ARIMA

C.P.Anil Kumar, Sarvesh Chandra and C. Selvaraj
Equatorial Geophysical Research Laboratory, Indian Institute of Geomagnetism, Krishnapuram, Tirunelveli, Tamil Nadu, India – 627011
&
J.Arul Asir and H.J.Jeyakumar
Pope's College, Swayearpuram, Manonmaniam Sundaranar University, Tirunelveli, Tamil Nadu India - 627012

Abstract
The atmospheric electric field (AEF) is a key parameter in the Global Electric Circuit (GEC) and plays a critical role in the performance of modern technological systems, particularly in aviation. In this study, we investigate the ambient variations in AEF during fair-weather conditions, using data collected from an electric field mill (EFM) over a period from 2020 to 2024. The data does not exhibit distinct frequency spectra, which necessitated the application of the Autoregressive Integrated Moving Average (ARIMA) method for effective pattern recognition. To evaluate the efficacy of the ARIMA model, minute averaged data spanning 2020 to 2022 were used. For predictive purposes, hourly averaged data from 2023 were employed to train the model and reduce its false alarm rate, enhancing its accuracy for future predictions and validated against 2024 data to assess its generalization capability. The ARIMA framework enables both short-term forecasting and analysis of long-term temporal patterns in AEF dynamics. With the application of ARIMA modelling more nuanced understanding of the spatio-temporal dynamics of AEF processes can be studied. These achievements pave the way for more accurate forecasting of AEF impacts on critical aviation technological infrastructure.

Date of Submission: 10-05-2025 Date of acceptance: 21-05-2025

I. Introduction

In 1860, Lord Kelvin conducted pioneering studies to investigate the Earth's electric field, laying the groundwork for the modern field of atmospheric electricity. Building on these efforts, Kennelly, 1902 proposed the existence of an electrically conductive layer in the upper atmosphere. He further noted that a spherical capacitor is formed between the Earth's surface and this conductive ionospheric layer (Rycroft et al., 2012). At the beginning of the 20th century, a series of experimental and observational studies, particularly those by Aplin and Harrison (2013), further developed the discipline, thereby establishing a new branch of Physics known as Atmospheric Electricity. Extensive land- and sea-based measurements by researchers revealed that the average electric potential of the upper atmosphere (ionosphere) is approximately 230 kV, Ralph Markson (1978). This value, however, exhibits temporal and spatial fluctuations even on fair-weather days, mainly influenced by global lightning activity and heliospheric processes (Kasemir, 1955; Chalmers, 1967; Kamra, 2001; Raina, 2002; Panneerselvam et al., 2007; Anil et al., 2008, 2009; Rycroft et al., 2012; Akhila and Anil, 2020)

A fair-weather day, in the context of atmospheric electricity, is defined as a day without precipitation, with wind speeds below 5 m/s, and cloud coverage less than 3 octas. Under such conditions, the vertical electric potential gradient (F), is related to the electric potential (V), vertical distance (h) from Earth's surface, conductivity (σ), and the permittivity of free space ε_0 as given in Eq. (1):

$$F = dV/dh \quad , \quad F = -\sigma/\varepsilon \qquad (1)$$

Specialized voltmeters known as electrometers are widely used to measure this potential difference at various altitudes (Rycroft et al., 2012 and references therein). Observations during fair-weather conditions have revealed not only a diurnal cycle in the electric field but also transient variations arising from the movement of space charges and electrified clouds. These space charges, transported by small, medium, and large ions, vary based on local wind conditions and prevailing weather. Their accumulation, often attributed to conductivity gradients, results in a net space charge density ρ, which is related to the potential gradient by Eq (2):

$$\rho=-\varepsilon_0 (df/dh) \quad (2)$$

Further research in AEF,, during fair weather observations indicated, diurnal variation, variations due to the movement of space charge of the lowest layers of the atmosphere and electrified cloud movements. Space charges are carried by small ions, medium ions and large ions, depends upon ambient wind condition and weather of the region. Overall process can be taken to be a pileup of charges due to conductivity gradient. Next, the density of space charge ρ is related to the potential gradient as $-\rho=\varepsilon_0 (d^2V/dh^2$, (Rycroft et al., 2012 and references cited therein). While long-term investigations agree well with the Carnegie curve, (Ralph Markson, 1978), short-term investigations have indicated considerable deviations from this standard curve (Clayton and Polk, 1977).

Multiple investigations have been conducted across the Indian subcontinent under varying meteorological, geophysical, and space-weather conditions (Kamra et al., 1997; Dutta and Bhattacharya, 2004; Kar et al., 2004; Anil Kumar et al., 2009, 2013). For instance, Kamra et al., (1997) focused on the impact of relative humidity on marine air conductivity; and Dutta and Bhattacharya (2004) examined electrical behavior during severe meteorological disturbances. Panneerselvam et al. (2007) analyzed the diurnal variation of Maxwell current over low-latitude tropical stations. Anil et al., (2009) measured conduction current in different meteorological condition density using an improved Wilson plate antenna, and later (2013) investigated changes in electrical parameters during the solar eclipse of 15 January 2010. A significant drop in aerosol loading cause substancial reduction in columnar resistivity during the COVID-19 lockdown was also reported (Anil et al., 2020).

We have been conducting long-term monitoring of atmospheric electrical parameters at Tirunelveli (8.70°N, 77.80°E), India, for over two decades. These studies are supplemented with automatic weather station (AWS) data to understand interconnections and teleconnections between meteorological and atmospheric electrical regimes (Anil et al., 2017).

Measurement of negative state of electric fields under fair-weather conditions is essential for understanding the fundamental processes governing the atmospheric electrical state. Since no active charge separation occurs during fair weather, these conditions provide a unique window into background electrical activity. Recently, compact Electric Field Mills (EFMs) have been widely adopted for high-resolution electric field measurements. These instruments measure the integrated electric field over an area roughly 25 km wide, with a sampling rate of one second and a resolution of 5 V/m (further details are provided in the instrumentation section).

To forecast future atmospheric electric field variations, we employ time series modelling techniques, including ARMA and ARIMA, which utilize past values and patterns for predictive purposes. For model development and evaluation, minute-averaged data from 2020 to 2022 were used. Hourly averaged data from 2023 and 2024 were then employed to refine the model, reducing false alarm rates and enhancing predictive accuracy.

II. Orography and Instrumentation

The measurement site is located in Krishnapuram village, situated at an elevation of 36 meters above mean sea level (AMSL). This remote location is characterized by minimal human habitation and a near absence of industrial activities. The area lacks major sources of anthropogenic aerosols such as quarrying, mining, cement production, and significant vehicular emissions. Additionally, the sparse presence of buildings and construction activities ensures low local aerosol loading, thereby providing a unique, uncontaminated environment, conducive to atmospheric measurements. Continuous observations have been conducted at this site since 1997.

The local terrain is predominantly rocky with minimal sandy features, and the region receives scanty rainfall due to its location in the rain shadow of the Western Ghats. To eliminate corona current arising from pointed vegetation, wild grass in the vicinity of the instrumentation has been systematically cleared. The experimental site lies approximately 35 km inland from the Gulf of Mannar, and the nearest urban centers Tirunelveli and Palayamkottai are situated 14 km and 12 km away, respectively. This geographical isolation ensures minimal influence from urban anthropogenic pollution.

Earlier studies (Panneerselvam et al., 2003, 2007; Anil Kumar et al., 2009, 2013, 2022) have confirmed the suitability of this location for high-fidelity atmospheric electricity measurements. Typically, experiments are carried out during the dry winter months from December to June, when fair-weather conditions prevail. The remaining part of the year is often dominated by adverse weather due to the monsoonal influence over the southern peninsular region of India.

In this study, we present hourly averaged data of fair-weather atmospheric electric field, complemented by concurrent measurements of key meteorological parameters. The unique low-aerosol environment and meteorological stability during the observation period make this dataset particularly valuable for studies in atmospheric electricity and related processes.

Electric fields in the atmosphere are established whenever there exists a gradient in electric potential. To quantify these fields with high precision, a specialized electro-mechanical instrument known as the Electric Field Mill (EFM) was employed at the measurement site. The deployed EFM is an upward-facing device constructed from non-magnetic stainless steel, ensuring long-term durability and electromagnetic neutrality in the presence of ambient fields.

The EFM operates based on the principle of electrostatic induction. The core sensing assembly comprises two electrodes: a stationary sensing electrode and a rotating shutter (or vane) mechanism that cyclically exposes and shields the sensing electrode from the ambient electric field. As the rotor modulates exposure to the atmospheric electric field lines, a time-varying surface charge is induced on the sensing electrode. This time-varying signal results in an alternating current that is directly proportional to the strength of the vertical electric field.

The induced current is collected by a secondary electrode and routed to a high-input impedance charge amplifier for signal conditioning. The amplified signal is subsequently digitized and transmitted to a data acquisition system through a multiplexer. Notably, the measured signal is independent of the rotor frequency, making the system robust against mechanical variation in rotational speed.

Calibration of the EFM was performed using the electrostatic relation E=V/dE = V/dE=V/d, where V is the known potential applied to a horizontal reference plate placed at a known vertical separation d (1 meter in this case) from the sensing head, as illustrated in Figure 1. The calibration procedure was carried out under controlled conditions to ensure traceability and accuracy. Proper electrical grounding, the use of high-reliability (military-grade) components, and optimized cabling and shielding configurations were implemented to eliminate parasitic currents, reduce noise, and minimize measurement uncertainty.

EFM instrumentation is described in further detail at http://www.boltek.com, including manufacturer specifications and system integration guidance.

Atmospheric electric potential (AEP) measurements are significantly influenced by boundary-layer meteorological processes. Incoming solar radiation initiates a suite of photochemical and thermodynamic interactions that govern tropospheric dynamics (Arnold et al., 1984; Castleman et al., 1971; Eisele, 1988; Hoppel et al., 1986; Jonassen and Wilkening, 1965; Junge, 1963; Mani and Huddar, 1972; Alderman and William, 1996). Therefore, synchronous recording of meteorological parameters is essential for interpreting EFM data within the context of fair-weather atmospheric electricity.

To this end, an Automated Weather Station (AWS) was deployed at the site. The AWS continuously monitors key atmospheric parameters including air temperature, relative humidity, atmospheric pressure, wind speed, and wind direction. Complementary to automated data acquisition, fair-weather observables such as cloud cover, precipitation status, and visibility were recorded manually throughout the experimental period to ensure compliance with fair-weather measurement protocols.

The observed meteorological conditions adhered strictly to fair-weather criteria and are summarized in Table 1. These auxiliary data are critical for distinguishing fair-weather electric field signatures from transient disturbances due to local convective activity or cloud electrification processes.

Figure 1. Electric Field Mill located in Equatorial Geophysical Research Laboratory (Tirunelveli)

III.Data used in this work and Methodology

The electrodynamical state of the low-latitude ionosphere is well-known to be equipotential during fair-weather days; thereby, providing the sequential opportunities to measure the regional impact of atmospheric electric field (AEF). The initial data selection process involved the assessment of a weather sheets that contains manual Nephological observations and AWS data to filter out any disturbances owing to the weather (Table1). We have excluded the periods of high clouds of more than 3 octas, wind speed of more than 5 m/s, and days with precipitation. We also rejected the intervals of saturated and excessively turbulent data due to unknown reasons. Based on these, the each resultant fair-weather day data comprising second samples data points from 2020 to 2024 were selected for further analysis. Such a strict data selection procedure resulted in 10 fair-weather days from 2020, 25 fair weather days from 2021, 15 fair weather days from 2022, 36 days of fair-weather data in 2023 and 28 fair weather days from 2024, respectively, tabulated in Table 1. Next, we carried out one minute averaging and hourly averaging of data. The observations are grouped into three categories namely, type I pattern and type II pattern; and continues fair weather days of 2023 and 2024 for forecasting study. We used time series analysis method. This classical statistical method assume that observations are independent and parameters are identically distributed, but varies over time. The complexities involved can be addressed through the application of appropriate mathematical /statistical techniques. In time domain approach the correlation between adjacent values is best explained by a dependence of the current value on past value, thus auto correlation function can be used for modelling a future value of the time series. This is a parametric approach. Further trends and seasonality are not represented by this deterministic function, so later different assessments about the role of stochastic movements with respected to this fact are consider (see, Kirchgassner, 2013). ARIMA is a popular statistical tool used for time series forecasting in Science

The Auto-regressive Integrated Moving Average (ARIMA) model is a statistical method for time series analysis, incorporating three fundamental components: Autoregressive (AR), Integrated (I), and Moving Average (MA). The AR model was initially introduced by Yule (1927) and later generalized by Walker (1931), while the MA model was first developed by Slutzky (1937). Wold (1938) subsequently provided the theoretical foundation for the combined Auto-Regressive Moving Average (ARMA) process. The ARIMA model, as extensively applied by Box and Jenkins (1970), integrates these elements to effectively analyze and forecast time series data. ARIMA models are a class of complex linear models capable of representing both stationary and non-stationary time series. Unlike regression models that incorporate independent variables, ARIMA models rely solely on the internal structure of the time series data for forecasting. Specifically, AR and MA models are suitable for stationary time series, whereas Integrated (I) models are necessary to address non-stationarity. ARIMA and SARIMA models are additions of ARMA model to include more accurate dynamics, i.e., non-stationarity in mean and seasonal patterns.

The Auto Regression (AR) component assumes that the data is dependent on its own lagged values. The (AR) part expresses the current value of the time series as a linear function of its past values i.e. the past values of the time series are used to predict the future value. The AR part of the model is denoted as (ARp) of order p, meaning that it uses the past p observations to predict the current value. The Integration part accounts for the differencing needed to make the time series stationary. The Integration component of the ARIMA model is responsible for making the time series stationary. A stationary time series has constant mean, variance, and auto-covariance over time, which is an essential assumption for many time series models. If a time series is non-stationary, it often exhibits trends or seasonal patterns that can distort the analysis. The differencing of the time series, involves in subtracting the previous observation from the current one. This process is repeated until the time series becomes stationary. The number of differencing operations required to make the series stationary is denoted by (I_d) of order d. The Moving Average (MA) part, models the relationship between the current value of the series and past forecast errors (or residuals). Unlike the AR part, which depends on past observations, the MA part relies on the errors in the prediction of the past values. The MA component incorporates past forecast errors to refine the model's predictions. The MA model assumes that the noise or randomness in the time series follows a random process and that past errors contribute to the current value. This component is particularly useful for modelling irregular fluctuations that cannot be explained by past values but are systematic in nature. The MA part of the model is denoted (MA_q) of the order q. When combined, the AR, I, and MA components form the ARIMA model the ARIMA model is represented as ARIMA (p,d,q). Hyndman and Athanasopoulos (2014): Pal and Prakash (2017): Naveen and Anu et al. (2017). The general form of the ARIMA (p, d, q) Eq.(3):

$$Y_t = C + \sum_{i=1}^{p} \phi_t y_{t-i} + \sum_{J=1}^{q} \theta_j \varepsilon_{t-j} + \varepsilon_t \qquad (3)$$

where c - is the constant term, Φ_t - is the coefficient of AR, θ_j - is the coefficient of MA

Table 1. Number of fair-weather days considered for the study during the years from 2020 to 2024

Date	Avg temp	Mean wind speed	Wind direction	Mean humidity	Cloud coverage	Max. visibility
09/1/2020	24	3m/s	Easterly	74%	3octas	10km
15/1/2020	26	5m/s	Easterly	74%	2octas	12km
19/1/2020	25	2m/s	Easterly	74%	2octas	12km
11/2/2020	24	3m/s	Westerly	71%	3octas	14km
17/2/2020	25	4m/s	Easterly	71%	3octas	12km
18/2/2020	26	2m/s	Easterly	71%	3octas	12km
19/2/2020	28	4m/s	S-W	71%	2octas	13km
15/3/2020	30	4m/s	S-W	67%	3octas	14km
16/4/2020	34	3m/s	Easterly	65%	2octas	14km
04/5/2020	36	4m/s	S-W	60%	2octas	14km
19/01/2021	26	3m/s	N-W	72.5%	3octas	10km
24/01/2021	25	3m/s	Easterly	72.8%	3octas	11km
25/01/2021	25	2m/s	Easterly	73.7%	3octas	10km
27/01/2021	26	4m/s	N-W	66.7%	3octas	12km
28/01/2021	25	2m/s	N-W	67%	3octas	12km
07/02/2021	22	3m/s	Easterly	69%	2octas	11km
08/02/2021	24	3m/s	Easterly	70.2%	3octas	12km
09/02/2021	24	4m/s	Easterly	73.9%	3octas	13km
10/02/2021	26	2m/s	Easterly	69.3%	3octas	12km
11/02/2021	25	2m/s	Easterly	70.8%	3octas	14km
12/02/2021	26	3m/s	Easterly	68.2%	2octas	13km
16/02/2021	25	3m/s	N-W	69.1%	3octas	12km
17/02/2021	27	2m/s	N-W	73.2%	3octas	13km
18/02/2021	27	4m/s	N-W	71.9%	2octas	10km
19/02/2021	24	4m/s	Westerly	68.2%	3octas	14km
26/02/2021	26	3m/s	Westerly	70.3%	3octas	12km
28/02/2021	26	3m/s	N-W	70%	2octas	13km
02/03/2021	27	4m/s	Easterly	59.9%	2octas	12km
03/03/2021	26	2m/s	Westerly	66.3%	2octas	12km
04/03/2021	23	2m/s	S-W	64%	2octas	11km
05/03/2021	24	3m/s	S-W	60%	2octas	12km
07/03/2021	24	3m/s	S-W	70.1%	3octas	13km
15/03/2021	26	5m/s	S-W	71.2%	3octas	12km
16/03/2021	27	5m/s	S-W	69.6%	2octas	14km
21/03/2021	29	4m/s	Variable	72.9%	1octas	13km
05/01/2022	26	3	N-E	60%	Clear sky	10km
09/01/2022	27	2	Easterly	56%	3octas	12km
20/01/2022	27	2	N-E	58%	2octas	10km
21/01/2022	28	3	N-E	60%	3octas	11km
01/02/2022	28	3	Easterly	52%	2octas	10km
02/02/2022	27.5	2	Easterly	54%	2octas	12km
03/02/2022	26.2	2	Easterly	50%	3octas	10km
05/02/2022	25	3	Easterly	57%	2octas	8km
23/02/2022	28	2	N-E	60%	3octas	9km
06/03/2022	27	2	N-E	62%	2octas	9km
09/03/2022	25	2	Easterly	59%	2octas	10km
15/03/2022	27	3	N-E	58%	2octas	10km
21/03/2022	26	3	Easterly	54%	2octas	12km
27/03/2022	25.5	2	S-W	57%	2octas	12km
28/03/2022	26	3	S-W	52%	1octas	13km

03/01/2023	23	2	Easterly	71%	Clear sky	8km
05/01/2023	24	3	Easterly	80%	Clear sky	9km
12/01/2023	26	2	N-E	75%	Clear sky	8km
13/01/2023	27	3	N-E	72%	Clear sky	10km
14/01/2023	27	2	N-E	62%	Clear sky	9km
15/01/2023	28	3	Easterly	64.4%	Clear sky	8km
16/01/2023	26	2	Easterly	62&	1 octas	9km
17/01/2023	24	2	Easterly	59%	2octas	9km
18/01/2023	24	3	Easterly	57%	2octas	10km
19/01/2023	25	2	Easterly	46%	2octas	9km
07/02/2023	28	3	Easterly	49%	2octas	11km
08/02/2023	27	3	Easterly	50%	Clear sky	10km
09/02/2023	26	2	Easterly	56%	Clear sky	12km
12/02/2023	27	2	Easterly	59%	1octas	10km
13/02/2023	28	3	Easterly	58%	2octas	9km
16/02/2023	27	2	Easterly	54%	2octas	10km
17/02/2023	27.5	2	Easterly	63%	3octas	10km
18/02/2023	26.3	3	Easterly	47%	2octas	10km
18/02/2023	27.5	3	Easterly	60%	4octas	11km
20/02/2023	26	2	Variable	60%	2octas	12km
21/02/2023	26.5	4	Variable	64%	3octas	11km
22/02/2023	27	3	S-W	57%	2octas	12km
23/02/2023	26	3	S-W	62%	3octas	9km
24/02/2023	26	4	Variable		2octas	10km
25/02/2023	27	3	Easterly		2octas	11km
26/02/2023	28	3	Easterly		3octas	12km
01/03/2023	27	2	Easterly		2octas	10km
02/03/2023	26.5	2	N-E		3octas	9km
03/03/2023	25	3	N-E		3octas	11km
04/03/2023	27	2	N-E		3octas	12km
05/03/2023	27	2	Easterly		2octas	10km
10/03/2023	28	3	Easterly		3octas	9km
11/03/2023	28	2	Variable		3octas	11km
12/03/2023	27.5	4	Easterly		Clear sky	10km
13/03/2023	27.9	2	N-E		1octas	11km
15/03/2023	29	4	Easterly		2octas	10km
29/01/2024	30	2	Easterly	64%	Clear sky	10km
30/01/2024	31	3	Easterly	62%	Clear sky	10km
07/02/2024	30.3	2	Easterly	60%	Clear sky	12km
08/02/2024	30.5	3	Easterly	64%	Clear sky	12km
12/02/2024	30.2	3	Easterly	62%	Clear sky	11km
13/02/2024	30.6	2	Easterly	64%	Clear Sky	12km
16/02/2024	32	2	N-E	68%	2	9km
19/02/2024	30.4	3	N-E	65%	3	10km
20/02/2024	30.6	2	N-E	67%	2	10km
21/02/2024	32	2	Easterly	56%	2	12km
22/02/2024	28	1	N-E	58%	3	11km
23/02/2024	30.5	1	Variable	57%	2	11km
24/02/2024	30	2	Variable	62%	2	12km
25/02/2024	32	2	N-E	54%	2	13km
26/02/2024	31	2	N-E	52%	3	11km
27/02/2024	33.5	3	N-E	53%	3	12km
28/02/2024	32	3	Easterly	53%	3	11km
29/02/2024	33	1	Easterly	52%	3	13km
07/03/2024	30.3	2	Easterly	50%	2	10km
08/03/2024	31	2	N-E	48%	clear sky	11km
11/03/2024	34	1	Variable	52%	clear sky	12km

20/03/2024	36	2	S-W	52%	2	12km
28/03/2024	35	3	S-W	55%	2	12km
29/03/2024	34	3	S-W	51%	3	12km
30/03/2024	38	2	S-W	50%	3	12km
31/03/2024	38	3	S-W	46%	2	11km
01/04/2024	35	2	S-W	45%	3	13km
02/04/2024	36	3	S-W	46%	1	13km

IV.Results & Discussion

ARIMA is a parametric modelling which provides a good forecasting to enhance the predictions. The suitable order of model is determined by the minimum value of Akaike Information Criterion (AIC). The observations from 2020 to 2022 mainly used for in-sample prediction and 2023 for training the model and 2024 data is utilized for out of sample forecast. For non-fairweather days Fast Fourier Transform method is mainly used to analyze and characterize AEF (see, Xiong and Chen, 2024, Anil et al. 2024).

For the year 2020 autocorrelation graph is shown in Fig 2(a) and partial autocorrelation graph is depicted in Fig 2(b). When data has a trend the autocorrelations function (ACF) for small lags tends to be large and positive because observations nearby in time are also nearby in size. While the partial autocorrelation function (PACF) convey the vital information regarding the dependence structure of a stationarity process. The partial auto correlation function of a time series quantifies the direct relationship between observations at different lags, by removing the influence of intermediate lags. The negative value of PACF is often called reflection coefficient. By the nature of correlations, reflection coefficient are always between -1 to +1 , Piet (2006).

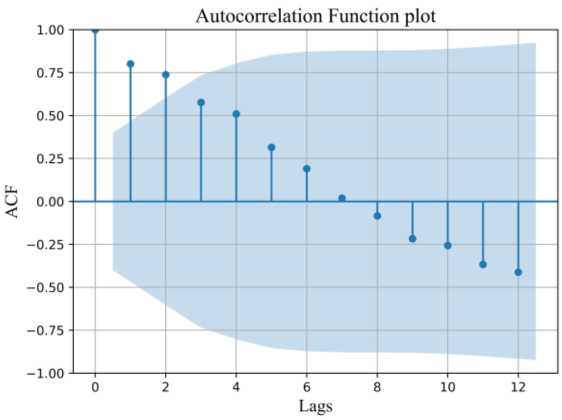

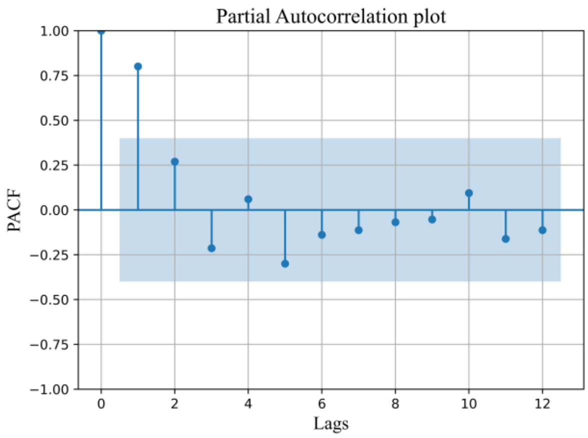

Fig 2(a). Represent ACF analysis of AEF 2020. **Fig. 2(b).** Represent PACF plot of 2020

Table 2. Selected order of AICs and BIC along with other statistical parameters.

Year	Model (p,d,q)	No. Observations	AR L1	AR L2	MA L1	AICs	BIC	HQIC	Constant Interceptor	Sigma^2	Ljung-Box	Jarque-Bera	Skew	Kurtosis
2020	(2,0,1)	24	0.2491	0.4972	0.4972	231	237	233	-82.5181	471	0.66	3.29	0.05	4.81
2021	(1,0,1)	24	0.0159	0.5998	0.2143	220	224	221	-151.2266	484	0.01	1.07	0.52	3.03
2022	(2,1,1)	24	0.3808	0.0232	0.6463	226	231	227	-139.1480	463	0.07	1.39	0.50	4.07
2023	(1,0,2)	96	0.5902	--	0.1015	100.1	101.4	100.6	-58.67	1777	0.01	2.97	0.11	5.72
2024	(1,1,3)	168	0.6341	--	0.103	165	167	166	-106.34	1021	0	3.5	0.59	4.92

Figure 3, depicts the results for the year 2020 ARIMA model. Table 2 indicates various diagnostic and statistical metrics, here p = 2, q = 0, d =1. The coefficients of the lag-1 and lag-2 of autoregressive terms are 0.2491, 0.4972 and moving average term is 0.4972 respectively. 231 is the lower value of AIC (Akaike Information Criterion) indicate a better model fit. BIC (Bayesian Information Criterion) is 237 similar to AIC but includes a penalty for more parameters. Next, model selection criterion is HQIC (Hannan-Quinn Information Criterion) =233, which balancing fit and complexity. -82.51V/m is the intercept term of the model. Sigma^2 is the estimated variance of the residuals. Ljung-Box Test (Ljung-Box statistic) is 0.66. This tests for autocorrelation in the residuals, is Jarque-Bera Test, which test for normality of the residuals; larger values indicate a deviation from normal. Skew = 0.05 is a measure of the asymmetry of the residual distribution; where a value close to 0 suggests symmetry. And Kurtosis is

4.81, a measure of the "tailedness" of the residual distribution; values close to 3 indicate a normal distribution (Pal and Prakash, 2017;Hyndman and Athanasopouos, 2014; Gautham and Singh 2020).

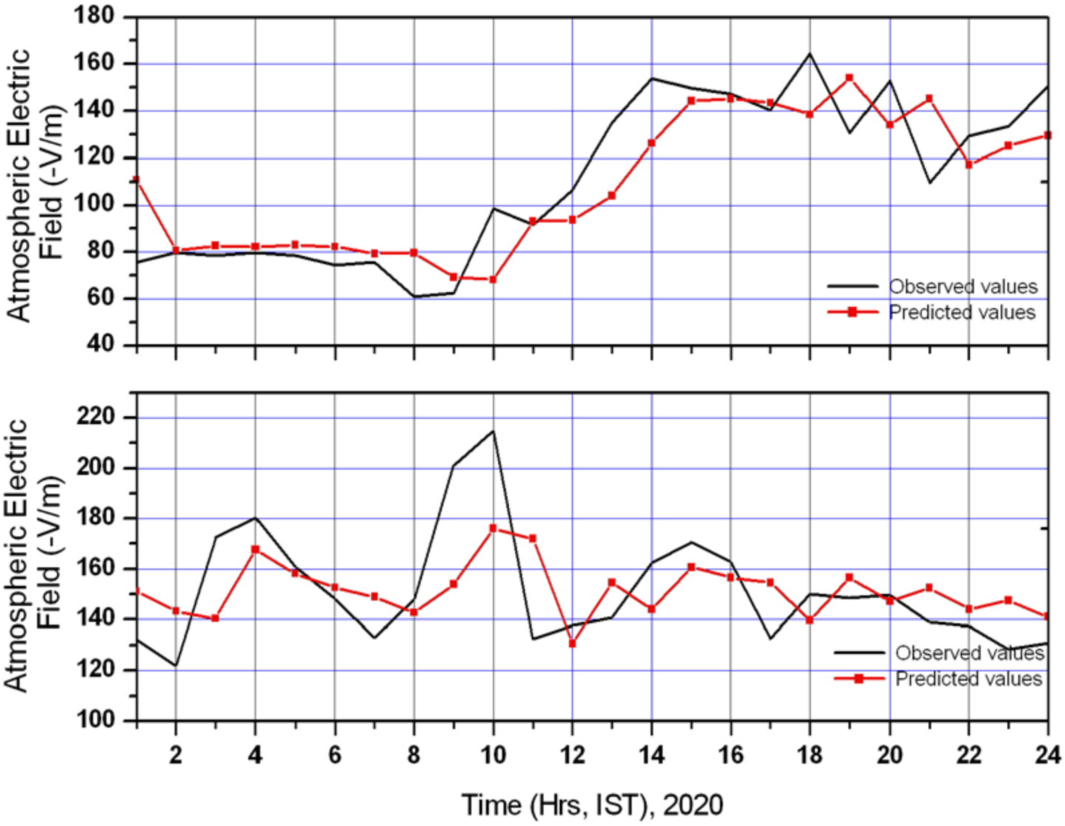

Fig 3. Observed AEF v/s in-sample predicted AEF for Tirunelveli, 2020

Fig. 3 (top) and (bottom) illustrates the two general observed pattern of AEF during 2020, these same-seasonal fair weather days (see, taken from Table 1) and their in-sample prediction of AEF during the year are fairly well predicted.

The ARIMA model for the year 2020 seems to have a good fit based on the AIC, BIC, and HQIC values as in Table 2. The Ljung-Box test statistic is low (0.66), suggesting that the residuals are not auto-correlated, which is a good sign for model validity. The skewness and kurtosis are fairly close to 0 and 3 respectively, which is close to a normal distribution, but the kurtosis value suggests the residuals have slightly heavier tails than a normal distribution. The (-82.51V/m) is the intercept of in this ARMA (better to say) model. It represents the baseline level of the time series when all AR and MA terms are zero. This can have important implications for understanding the underlying system.

The ARIMA (1,0,1) model for the year 2021 figure 4 (top and bottom) performs statistically sound and scientifically valid, making it a reliable choice for forecasting short-term trends in the given dataset observed. The values as in figure 4 however, the weak AR = 0.0159 autoregressive influence from previous time point and MA coefficients suggest the series may not have strong internal structure. The intercept term in the model equation influences baseline level (-151.23V/m) of the series. Here, the forecasting accuracy may be limited to short horizons. AICs =220, BIC =224 and HQIC =221 are less when comparing with other models values. This model was chosen based on being the lowest among tested configurations, it is likely the high likely hood model available. The diagnostics test indicate the model's residuals meet key assumptions. Model passes Ljung-Box, Jarque-Bera, skewness, and kurtosis checks, confirming it's valid for forecasting.

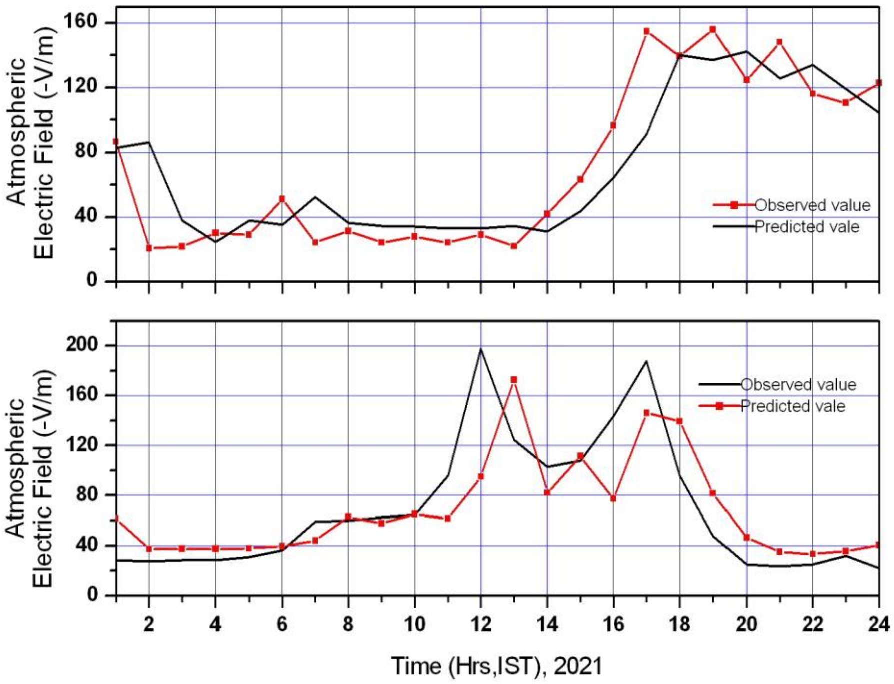

Fig 4. observed AEF v/s out sample trial of AEF for year, 2021

The results of ARIMA model with parameters (2,1,1) fitted to time series data for the year 2022. The model captured the underlying structure of the data in order to forecast future values and analyze key statistical properties such as autocorrelation, normality, and model fit. The selected ARIMA model has two autoregressive terms (p=2), one differencing term (d=1) to ensure stationarity, and one moving average term (q=1).The autoregressive coefficients, 0.3808 and 0.0232, indicate that the past two values of the time series influence the current value. The first lag (AR L1) has a more substantial impact, while the second lag (AR L2) is much smaller, implying diminishing relevance of past values beyond the first lag. The moving average coefficient 0.6463 suggests that past error terms have a significant influence on the current value of the time series. The positive value indicates that positive errors in previous periods have a direct impact on the value of the current observation. The intercept −139V/m of the model, indicating the baseline level around which the time series fluctuates. It suggests that, on average, the time series tends to be around -139.15, adjusted for the autoregressive and moving average effects.

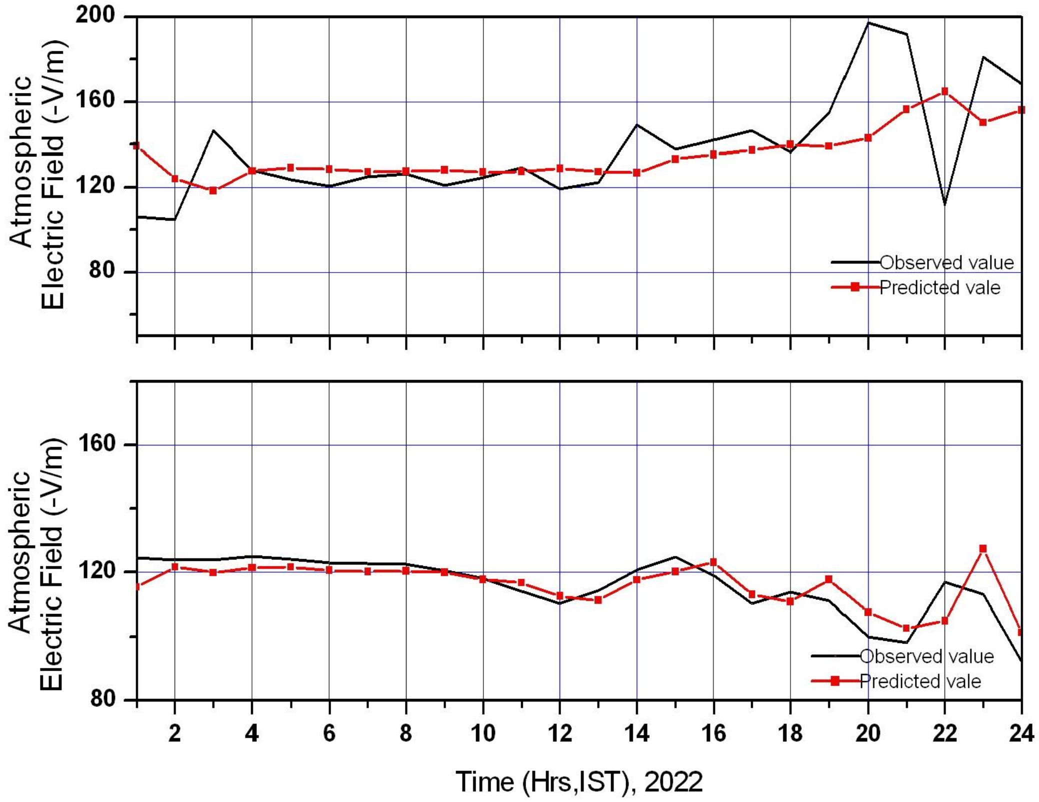

Fig 5. AEF actual v/s trial forecast of AEF for year , 2022

The model fit is evaluated using three commonly used information criteria: AIC =226 BIC=231 and HQIC=227. These fit indices are used to compare different models, where lower values indicate a better trade-off between model fit and complexity. In this case, the values of AIC, BIC, and HQIC are fairly close, suggesting that the model has balanced fit without over fitting. The relatively low values indicate that the model captures the data structure effectively while avoiding unnecessary complexity.

Ljung-Box test checks for autocorrelation in the residuals of the model. A low p-value indicates that there is significant autocorrelation left in the residuals, implying that the model may not have fully captured the underlying process. However, a value of 1.39 suggests no significant autocorrelation remains, indicating that the residuals are approximately white noise. The Jarque-Bera test assesses whether the residuals are normally distributed. The statistic of 0.50 suggests that the residuals are fairly normal, with no significant departure from normality. This implies that the model's residuals do not exhibit extreme skewness or kurtosis, and the assumption of normality is reasonable.

Figure 5 (top panel and bottom panels) with ARIMA model with (2,1,1) parameters fits the data reasonably well, as indicated by the low values of the AIC, BIC, and HQIC, and the satisfactory diagnostic test results. The Ljung-Box test suggests that there is no significant autocorrelation in the residuals, which is a good indicator that the model captures the temporal dependencies in the data effectively. The normality assumption is also reasonably satisfied according to the Jarque-Bera test, though the high skewness suggests that the model could potentially be improved by addressing the asymmetry of the residuals. In conclusion, the ARMA(2,1,1) model is effective in modeling the time series data for the year 2022. The model's fit statistics, diagnostic checks, and residual analysis suggest that the model captures the key characteristics of the data.

In figure 6, ARIMA(1,0,2) Model selection criteria values were AIC = 100.1, was fitted to a dataset comprising 96 observations from 1 to 4, April 2023. The autoregressive coefficient at lag 1 (AR1) was estimated at 0.5902, indicating a moderate level of persistence in the time series, while the first moving average coefficient (MA1) was 0.1015, suggesting a relatively minor correction for short-term shocks. Residual diagnostics showed no significancy, (Ljung-Box Q = 0.01), and the residuals were approximately symmetric (skewness = 0.11). However, the kurtosis value of 5.72 indicates a leptokurtic distribution, suggesting the presence of heavy tails and a higher-than-

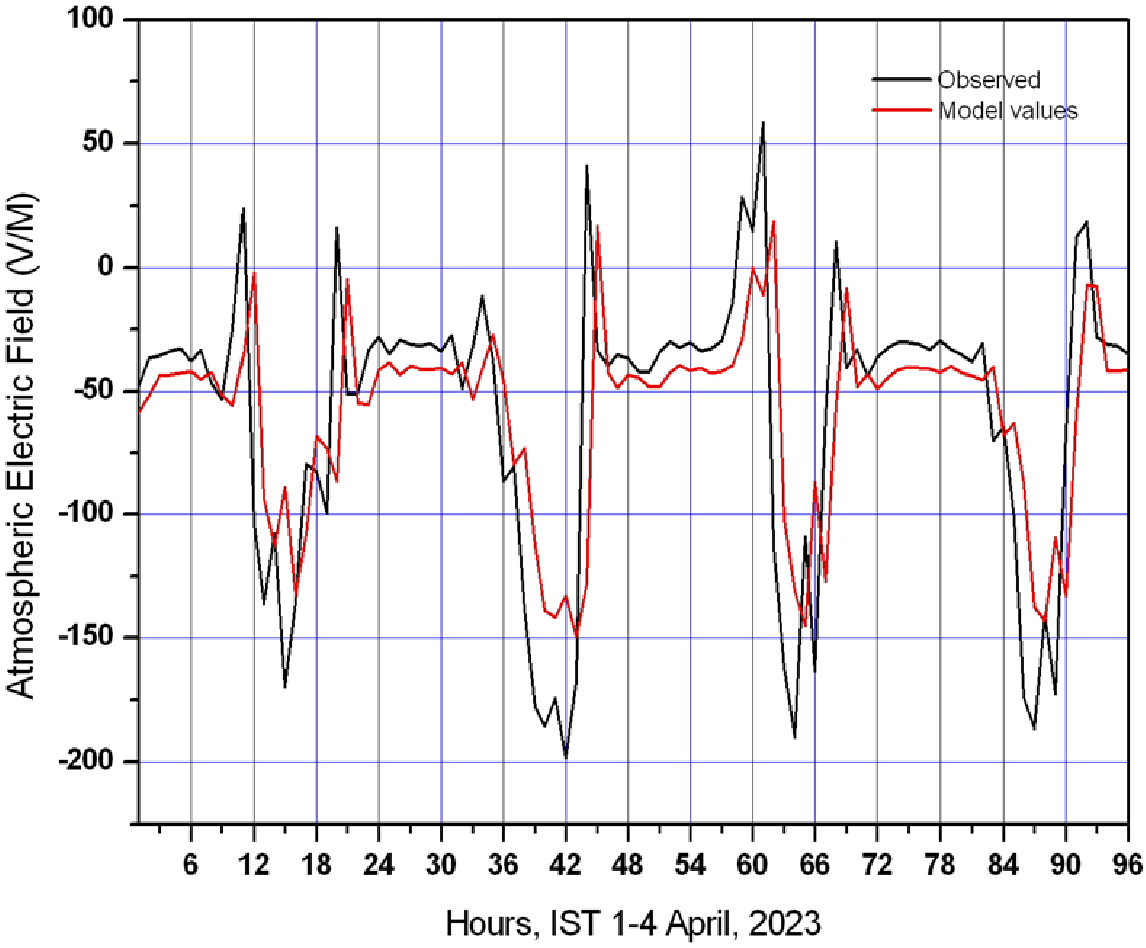

Fig 6. AEF actual v/s trial forecast of AEF for year , 2023

normal probability of extreme values. The Jarque-Bera test statistic (2.97) was below the 5% critical threshold, implying no strong evidence against normality, although the residual variance (σ^2 = 1777) remained high, pointing to a substantial amount of unexplained variability. Overall, while the model captures key dynamics in the data.

The time series analysis of the model (1,1,3) based on 168 observations in figure 7 provides important insights into the temporal dynamics of the datase, from 19 to 25, February, 2024. The autoregressive term (AR L1) is estimated at 0.6341, suggesting a significant degree of persistence, indicating that past values have a substantial influence on current outcomes.

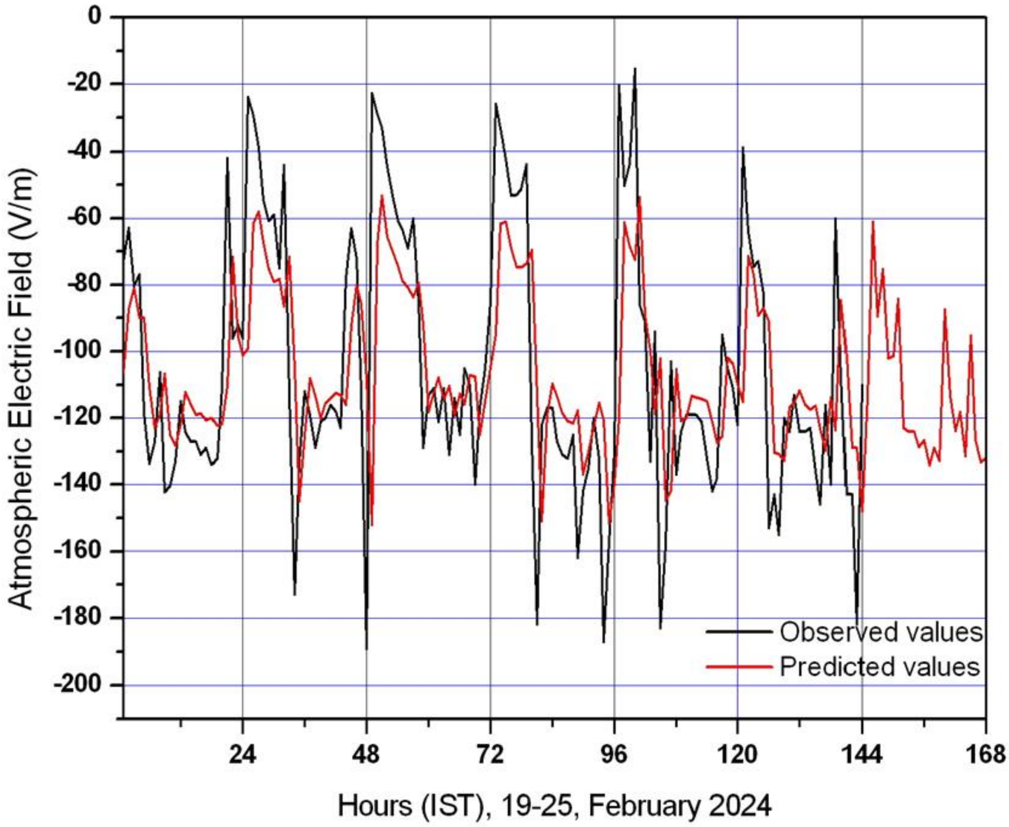

Fig 7, Time series analysis of the model (1,1,3) based on 144 observations of 2024 and forecast

In contrast, the first-order moving average term (MA L1) is lower at 0.103, implying that the impact of random shocks diminishes rapidly over time. The model's adequacy is evaluated through the Akaike Information Criterion = -106.34 and Bayesian Information Criterion = 1021, which promotes good model selection, though the BIC indicates potential over fitting. The absence of significant autocorrelation in the residuals, indicated by the Ljung-Box statistic, signifies a good fit. Overall, while the model effectively delineates the core characteristics of the time series for prediction Figure 7. The values from 144Hrs to 168Hrs (IST) is the prediction of this model.

The ARIMA model fits the data relatively well, with significant coefficients for the intercept and moving average term. The Ljung-Box test and Jarque-Bera test suggest that the residuals are fairly well-behaved.

VI. Conclusions

We developed an innovative approach to model AEF during fair-weather conditions by utilizing data collected from an Electric Field Mill (EFM) spanning from 2020 to 2024 and applied the ARIMA model. This parametric modelling method provides a good forecast to enhance the prediction. This is achieved through the auto-regressive integrated moving average and the model parameter is determined by the minimum value of Akaike Information Criterion (AIC). The observations from 2020 to 2022 mainly used for in-sample predictions. The model was trained on the 2023 dataset and validated against 2024 data to assess its generalization capability. The ARIMA framework enables both short-term forecasting and analysis of long-term temporal patterns in AEF dynamics. With the application of ARIMA modelling more nuanced understanding of the spatio-temporal dynamics of AEF processes can be studied. These achievements pave the way for more accurate forecasting of AEF impacts on critical aviation technological infrastructure.

References

[1]. Adlerman, E.J. and Williams, E.R., 1996. Seasonal variation of global electric circuit. J. Geophys. Res., 101, 29679-29688.

[2]. Akhila J. C. K. and C. P. Anil Kumar,2020, Investigation on High Velocity Plasmas and Field Aligned Currents at High Latitudes, Asian Journal of Research and Reviews in Physics3(2): 22-

29.https://doi.org/10.9734/ajr2p/2020/v3i230117

[3]. Anil Kumar, C.P., C.Panneerselvam, K.U.Nair, K.Jeeva, C.Selvaraj, S.Gurubaran, and R.Rajaram, 2008 Influence of coronal mass ejections on global electric circuit, Ind. J. Radio and Space Phys, 37, 39-45, 2008

[4]. Anil Kumar, C.P., Panneerselvam, C., Nair, K.U., Jeyakumar, H.J., Selvaraj, C. and Gurubaran, S., 2009. Measurement of atmospheric air-earth current density from a tropical station using, improvised Wilson's plate antenna, Earth Planet and Space, 61, 919-926.

[5]. Anil Kumar, C.P., Gopal Singh, R., Selvaraj, C., Nair, K.U., Jayakumar, H.J., Vishnu, R., Muralidas, S. and Balan, N., 2013. Atmospheric electric parameters and micrometeorological process during the solar eclipse on 15 January, 2010., J. Geophys. Res. (Atmos) 118, 5098-5104, doi:10.1002/jgrd.50437.2013.

[6]. Anil Kumar, C. P., Balan, N., Pannerselvam, C., Jeni Victor, N., Selvaraj, C., Nair, K.U., Elango, P., Jeeva, K., Akhila., J.C. and Gurubaran, S., 2017. Investigation of the Influence of Galactic Cosmic Rays on Clouds and Climate. Proc. Indian National Sci., Acadmy, 83, 631-644, doi: 10.16943/ptinsa/2017/49028, 2017, ISSN 2454-9983.

[7]. Anil Kumar, C. P., N.Venkatesh, C.Panneerselvam and C. Selvaraj, Measurement of Maxwell's current density from a tropical station during severe lightning disturbances and fair-weather days of 2019, 2020, J. Ind. Geophys.Union, 24(3), 25-31, 2020.

[8]. Anil Kumar,C.P.. C.Selvaraj, C. Panneerselvam, Sarvesh Chandra, J. Arul Asir and M.K.Sheriff, 2025, Analysis of intensified electric field jumps associated with the ASANI cyclone observed from Tirunelveli ($8^{0}.7^{'}$N, $77^{0}.8^{'}$E), Mousam (Revised)

[9]. Aplin, K.L. and Harrison, R.G., 2013. Lord Kelvin's atmospheric electricity measurements. Hist. Geo. Space Sci., 4 (2), 83–95.

[10]. Arnold, F.H., Heitmann and Oberfrank, K., 1984. First composition measurements of positive ions in the upper troposphere, Planet. Space Sci., 32, 1567-1576.

[11]. Box G E and G.M.Jenkins, 1976, Time series analysis: forecasting and control, revised edition, Hoilden-Day publications, San Fransico.

[12]. Burns, G.B., Frank-Kamenetsky, A.V., Troshichev, O.A., Bering, E.A. and Reddell, B.D., 2005. Interannual consistency of bi-monthly differences in diurnal variations of the ground level vertical electric field J. Geophys. Res. 110, D10106, doi:10.1029/2004JD005469.

[13]. Castleman, A., Tang, W.I.N. and Munkelwiz, H.R., 1971. Clustering of sulfur dioxide and water vapour about oxonium and nitric oxide ions., Amer. Assoc. Advanc. Sci., 173, 1025-1027.

[14]. Chaimers, J.A. 1967. Atmospheric electricity, Pergumon press, New York, 34-38.

[15]. Clayton, M. and Polk, C., 1977. Electrical Process in Atmospheres, Proc. 5th Int. Conf. on Atmospheric Electricity (Ed) Garmisch Partenkirchen, Dolezalek, H., and Steinkopt, R., 440-451.

[16]. Datta, T. and Bhattacharya, A.B., 2004. Atmosphericelectrical field in relation to severe meteorological disturbances. Ind. J. Radio and Space Phys., 33, 374- 383.

[17]. Eisele, F.L., 1988. First tandem mass spectrometric measurement of tropospheric ions, J. Geophys. Res. 93, 716-724.

[18]. Gautam Aand Singh V (2020), Parametric versus non-parametric time series forecasting methods:A review, Journal of Engineering Science and Technology Review, 13,3, 165-171, https://doi.org/10.25103/JESTR.133.18

[19]. Hoppel, W.A., Anderson, R.V. and Willet, J.C., 1986. Atmospheric electricity in the planetary boundary layer, The Earth electrical environment, 149-165, National academy press, Washington D.C.

[20]. Hyndman R J, and Athanasopoulos g, 2014, Forecasting : principles and practice.

[21]. Jonassen, N. and Wilkening, M.H., 1965. Conductivity and concentration of small ions in the lower atmosphere, J.Geophys. Res., 70, 779-784.

[22]. Junge, C.E., 1963. Air chemistry and radioactivity, Academic press., New York, 336-382.

[23]. Kamra, A.K., Deshpande, C.G. and Gopalakrishnan, V., 1997. Effect of relative humidity on the electrical conductivity of marine air. Q. J. R. Meteorol Soc. 123, 1295- 1302.

[24]. Kamra, A.K., (Edt), 2001. Cloud physics and atmospheric electricity frontiers, Vol-II, pages 696-875.

[25]. Kar, S.K., Bhattacharya, A.B. and Yuei-An Liou, 2004. Solar effects on terrestrial

radio communication disturbances and associated tropospheric and ionospheric variations. Ind. J. Phys. 78(B), 151- 163.

[26]. Kasemir, H.W., 1955. Measurement of the air-earth current density, in Proc. Conf. Atmos. Electricity, Geophys. Res. Pap., 42, 91-95, Air Force Cambridge Res., Cent., Bedford.

[27]. Kirchgassner, S and Wolters, 2013, Introduction to modern time series analysis,

[28]. Mani, A. and Huddar, B.B., 1972. Studies of the surface aerosols and their effect on atmospheric electric parameters, Pure Appl. Geophys., 100, 154-166.

[29]. Naveen V and Anu N (2017). Time series analysis to forecast A.Q.I in Thiruvananthapuram, Kerala, India, Int. Journal of Engineering Rsearch and Applications, 07, 06, 66-84, https:doi.org/10.9790/9622-0706036684.

[30]. Pal A, and Prakash P K S, 2017, Practical Time Seris nalysis: Mastering time series data, processing, visualization and modeling using Python., Pack Publishing Ltd.

[31]. Panneerselvam, C., Selvaraj, C., Jeeva, K., Nair, K. U., Anil Kumar, C. P., and Gurubaran S., 2007. Diurnal variation of atmospheric Maxwell current over the low latitude continental station, Tirunelveli. Earth Planets Space, 59(5), 429–435.

[32]. Panneerselvam, C., Nair, K.U., Jeeva, K., Selvaraj, C., Gurubaran, S. and Rajaram, R., 2003. A comparative study of atmospheric Maxwell current and electric field from a low latitude station Tirunelveli, Earth Planets Space, 55, 697-703.

[33]. Raina, B.N., 2002. Surface measurements of the components of air-earth current density. Cloud Physics and Atmospheric Electricity Frontiers, Vol. II, 973-988

[34]. Ralph Markson, W., 1978. Solar modulation of atmospheric electrification and possible implications of the sun –weather relationship, Nature, 273, 103-109.

[35]. Rycroft, M.J., Keri, A. Nicoll., Aplin K.A. and Harrison, R.G., 2012. Recent advances in global electric circuit coupling between the space environment and the troposphere, J. Atmos. and Solar Terr. Phys., 90-91, 298-311.

[36]. Slutzky, E. (1937). Summation of random causes as the source of cyclic processes, Econometrica, 5, 105–146.

[37]. Walker G (1931) On periodicity in series of related terms. Proc R Soc Lond Ser A 131(818):518–532

[38]. Wold, H. 1938: A Study in the Analysis of Stationary Time Series.Stockholm: Almqvist and Wiksell.

[39]. Xiong A, Xu H, and Chen Z, 2024, Frequency domain analysis of atmospheric electric field and thunderstorm forecasting, Electronics, Communications and Networks, https://doi:10.3233/FAIA231228

[40]. Yule G U 1927 On a Method of Investigating Periodicities in Disturbed Series, with Special Reference to Wolfer's Sunspot Numbers Phil. Trans. R. Soc. Lond., A, 226,267-298, 1927